# MSEC2019-2787

# GAUSSIAN PROCESS TENSOR RESPONSES EMULATION FOR DROPLET SOLIDIFICATION IN FREEZE NANO 3D PRINTING OF ENERGY PRODUCTS

Luis Javier Segura, Guanglei Zhao, Hongyue Sun<sup>1</sup>, Chi Zhou

Department of Industrial and Systems Engineering University at Buffalo, the State University of New York Buffalo, NY 14260, U.S.A.

#### **ABSTRACT**

Freeze nano 3D printing is a novel process that seamlessly integrates freeze casting and inkjet printing processes. It can fabricate flexible energy products with both macroscale and microscale features. These multi-scale features enable good mechanical and electrical properties with lightweight structures. However, the quality issues are among the biggest barriers that freeze nano printing, and other 3D printing processes, need to come through. In particular, the droplet solidification behavior is crucial for the product quality. The physical based heat transfer models are computationally inefficient for the online solidification time prediction during the printing process. In this paper, we integrate machine learning (i.e., tensor decomposition) methods and physical models to emulate the tensor responses of droplet solidification time from the physical based models. The tensor responses are factorized with joint tensor decomposition, and represented with low dimensional vectors. We then model these low dimensional vectors with Gaussian process models. We demonstrate the proposed framework for emulating the physical models of freeze nano 3D printing, which can help the future real-time process optimization.

**Keywords**: 3D Printing, Energy 3D Printing, Freeze Nano Printing, Gaussian Process, Tensor Response

### INTRODUCTION

The rapid development of smart devices, wearable sensors, and electric vehicle requires energy storage devices to be inexpensive, flexible, lightweight, and environmental friendly [1, 2]. There is also a great need for micro-devices with high energy density and high power density. However, as reported by U.S. defense logistics agency, the current energy storage materials and devices can have either high energy density or high

power density, but they do not have both properties [3]. 3D printing is a promising technique to increase the energy and power density within a small footprint by decreasing transport path of ions in the electrolyte [4]. 3D printing is able to fabricate parts layer by layer with fine resolution and has been widely used to produce customized products [5]. To date, various 3D printing techniques based on material extrusion (e.g., fused deposition modeling, FDM), material jetting (e.g., inkjet printing), powder bed fusion (e.g., selective laser melting, SLM), vat polymerization (stereolithography, SLA) are developed. Among these techniques, material extrusion and material jetting have been successfully demonstrated to print energy products, such as fuel cells and batteries, with good electrical properties [6-8].

Recently, a novel 3D printing technique, freeze nano printing, was developed to have both macroscale and microscale feature printing capabilities. Figure 1 shows a schematic illustration of the freeze nano printing process, which seamlessly integrates freeze casting and inkjet printing [9]. The process starts with the suspension design, such as graphene oxide (GO) suspension (Step 1). The individual droplets of the support structure and the suspension are ejected to a cold substrate through a nozzle to form the printed layers (Steps 2-3). In particular, the droplets are supplied by a piezoelectric that controls the demand of the aqueous solution. The water based GO suspension is frozen and the ice crystals are formed at an ambient temperature of -20°C. Once the part is 3D printed, it is immersed in liquid nitrogen at -190°C approximately (Step 4), freeze dried to remove water (Step 5), and finally it undergoes sintering or thermal annealing to obtain the ultralight 3D printed structure (Step 6) [9].

The freeze nano printing process has successfully printed supercapacitor with superior properties [10]. Similar to the previously demonstrated 3D printing examples, freeze nano

Copyright © 2019 ASME

<sup>&</sup>lt;sup>1</sup> Contact author: hongyues@buffalo.edu

printing can efficiently print flexible products within limited space. Due to the porous structure after freeze drying, the energy density of the freeze nano printing products is higher [9]. Moreover, different from the continuous inkjet technique to print graphene structures by adjusting the rheological properties of Graphene Aerogel (GA) inks, freeze nano printing uses a low viscous Newtonian GO suspension that allows printing droplet by droplet until the layers are formed. As a result, it has an improved bonding strength among layers [9].

The existing studies on 3D printing of energy products focus on proof-of-concept demonstration, but do not pay attention to the quality and repeatability of the printed products. Actually, the limited quality and high uncertainty are common challenges for 3D printing processes [11]. In the freeze nano printing process, a critical quality-determining factor is the droplet solidification time. It will affect the determination of waiting time among layers and subsequently affect the part bonding strength and geometrical accuracy. The waiting time will also affect the printing productivity. It is therefore of great importance to study the solidification time for best waiting time determination.

However, the droplet solidification study is a non-trivial problem since the complex thermal interactions among the droplets, substrate and ambient. In addition, the aqueous graphene suspension experiences phase change during the solidification, where the released latent heat prevents the deposited droplets to freeze and affects the macro- and microstructures. Furthermore, the solidification is also dependent on the process parameters (e.g., layer thickness) and material properties (e.g., heat transfer coefficient). It is impractical to study the droplet solidification and optimize the waiting time in a trial-and-error approach, since the graphene is a very expensive material (\$300/g). To attack this problem, physical based thermal models are proposed to model the droplet thermal interactions and solidifications [12]. These models can be further used for the waiting time determination [12]. However, the physical based models can be computationally inefficient to be executed online for the droplet solidification study and waiting time determination.

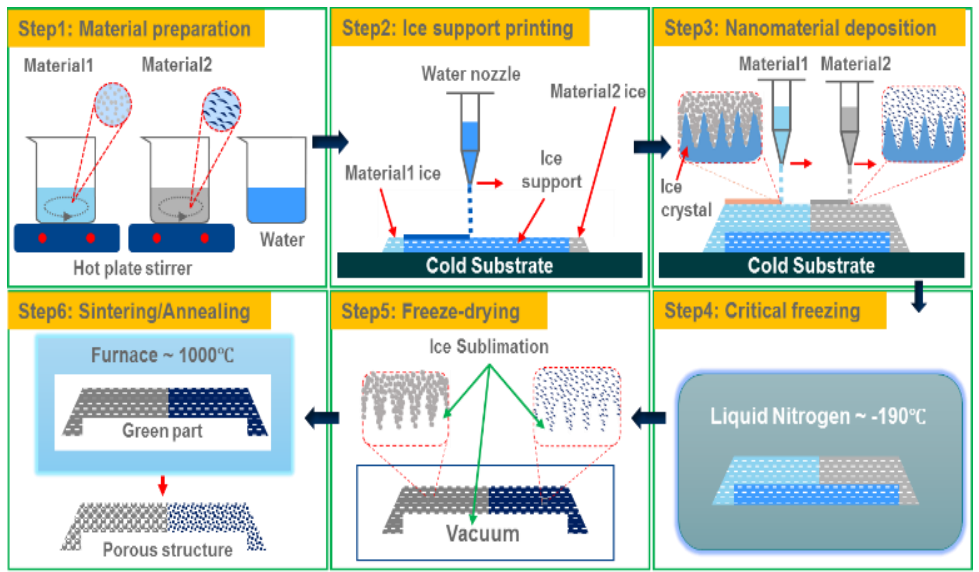


FIGURE 1. A SCHEMATIC REPRESENTATION OF THE FREEZE NANO 3D PRINTING PROCESS [9]

The objective of this work is to propose an efficient and accurate emulator for the physical model results of high dimensional droplet solidification time, so that this emulator can be used for the future online adjustment of waiting time and process parameters. To achieve this goal, we integrate machine learning techniques and physical models (see details in the Proposed Method section). In particular, we factorize the tensor responses at various process parameters with joint tensor decomposition so that the high dimensional responses are represented with low dimensional vectors. We then model the independent individual entries in these low dimensional vectors with Gaussian Process (GP) models. From the case study, this emulator can yield good prediction result, and can have very fast solidification time prediction. Such a model is applicable to the tensor responses modeling from the physical models, and can be

widely used for other 3D printing processes, such as the thermal simulation in SLM and droplet simulation in inkjet printing [13, 14]. To the best of our knowledge, this is the first paper for the modeling of the matrix or tensor responses in the physical models for 3D printing processes. In the future, we will investigate the application of the emulator for process optimization, and will also perform the thermal measurement from the printing process to calibrate the emulator.

The remainder of this paper is organized as follows. We review the related topics in the next section. After that, we provide a detailed description of the proposed method, and then elaborate the proposed method in a case study in the freeze nano printing process. Finally, we conclude the paper and discuss the future work.

#### STATE-OF-THE-ART

In this section, we first review relevant literature on the 3D printing of energy products, and then summarize the existing works on quality control of the 3D printed parts, and finally discuss the tensor response modeling works in manufacturing.

3D printing of anode, cathode and electrolyte, which are the main components in energy storage devices, has shown promising results towards increasing the performance of batteries and capacitors. Nevertheless, 3D printing of these components is not straightforward [9]. A Li-Ion microbattery architecture was developed in [15]. Interdigitated electrodes were integrated on a submillimeter scale, where Li<sub>4</sub>Ti<sub>5</sub>O<sub>12</sub> (LTO) and LiFePO<sub>4</sub> (LFP) were used as anode and cathode electrodes respectively. The ink design was optimized for composition and rheological behaviors to ensure reliable drops flow through the nozzles. The authors claimed the device vielded the highest areal energy and power densities reported to date. In another example, graphene oxide-based electrode inks for Li-Ion batteries were 3D printed [6]. To develop printable inks, the authors rely on Graphene Oxide's (GO) rheological properties, such as shear thinning behavior and high viscosity, as well as its exceptional electrical properties like high electrical conductivity, good structural stability and high surface area. Additionally, GO had shown potential to be used under this context due to its unique viscoelastic properties. Therefore, interdigitated GO-based electrode composite inks and solidstate electrolyte inks were used to 3D print anode, cathode, and electrolyte. The high areal surface due to the porous GO structure will increase the energy storage capacity. See also other examples in [7, 8].

Even though there are a lot of work related to 3D printing for energy storage devices, these efforts are at the proof-of-concept fabrication and the product integrity, quality and productivity have not been fully considered to the best of our knowledge.

Various 3D printing product defects are investigated via data-driven, physical based, or hybrid modeling approaches. For instance, porosity is a defect that compromises the mechanical properties, tensile strength, ductility and fatigue properties of the parts. The part average porosity was studied in SLM printing by a GP model to predict the porosity in the metal parts at any given combination of process parameters [16]. However, the authors did not consider the spatial distribution of porosity in the part. For another example, geometrical shrinkage affected the final dimension of a 3D printed part. A systematic model to predict part shrinkage and an optimal shrinkage compensation plan to achieve dimensional accuracy were presented in [17]. The model was validated using 3D printed cylinders by SLA, and it showed a significant dimensional improvement. See another example of the data driven modeling in [18]. Another kind of modeling is based on physical rules. For instance, the heat transfer in freeze nano printing was modeled in [12]. The heat transfer model was used to predict the temperature evolution of the printed droplets. The fluid dynamics was modeled for inkjet printing [19]. The model simulated the dispensing of polysiloxane via micro-syringe nozzle deposition, and could be used to solve the overfilling of materials at determined locations when trajectory change was present [19]. These models can be time consuming to be evaluated, and may also suffer from model uncertainty. To address these problems, the emulation/calibration models integrate the data-driven and physical rule based models. For instance, [20] used a functional GP model for the physical model calibration. See also [16]. However, the existing emulation/calibration models do not address the high dimensional matrix/tensor responses.

Recently, much attention was drawn to the tensor responses modeling. For instance, a regularized tensor regression was proposed for the turning process optimization [21]. The proposed method was applied to establish a relationship between the dimensional accuracy and process parameters by using high dimensional point cloud measurement of cylinder parts. Additionally, a method to quickly classify part geometrical integrity with minimal point cloud data in FDM was proposed in [22]. More information on the tensor responses modeling in manufacturing can be found in [23].

In this work, we integrate the joint tensor decomposition and GP model to handle the high dimensional responses from the physical models of freeze nano printing.

#### PROPOSED METHOD

To effectively represent and model the tensor outputs of droplet solidification time from the physical models, we propose to integrate joint tensor decomposition and physical models. Our ultimate goal is to build an efficient and accurate emulator for the prediction of droplet solidification time at new process settings, which can be used for the future online waiting time and process setting control.

Figure 2 shows our proposed analysis procedures. To investigate the freeze nano printing process (Figure 2 (a)), physical models are developed to characterize the droplets' thermal distributions [12]. Based on these physical models, we simulate the thermal distributions at the process settings specified by a computer design of experiment (details to be provided in the case study). We then summarize the droplet solidification time for each simulated process setting, as illustrated in an example in the bottom of Figure 2 (b). The solidification time at the droplets will form a tensor response. After that, as shown in the top of Figure 2 (c), the solidification time across different process settings are factorized by joint Candecomp/Parafac (CP) tensor decomposition. After the decomposition, the non-zero entries in the core tensors only reside on the diagonal (i.e., the core tensors are orthogonal, as shown in Figure 3). Therefore, we model each entry at a fixed coordinate of the core tensors from different process settings with a GP model. Since the core tensors are orthogonal, we can model each entry independently. Finally, after separately training the GP models, the droplet solidification time can be predicted by the reconstruction from the predicted core tensor entries and the factorization matrices. This reconstructed tensor will be compared with the droplet solidification time simulated from the physical models.

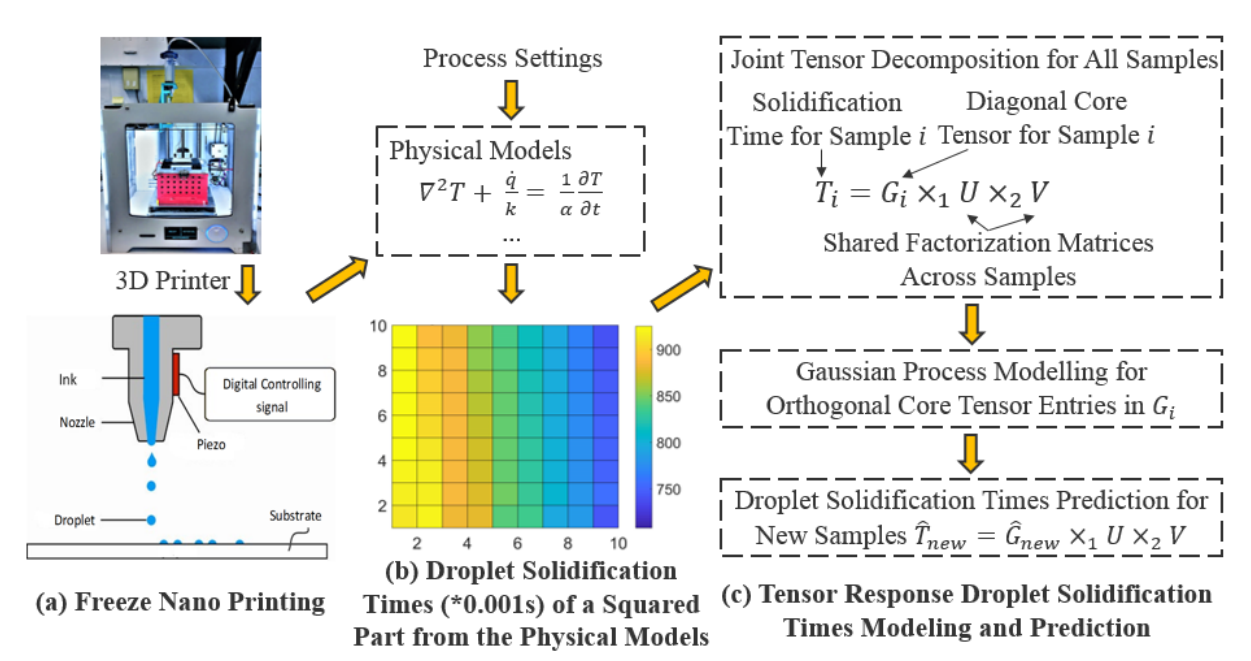


FIGURE 2. PROCEDURES IN THE PROPOSED FRAMEWORK

In the above procedures, the simulation data generation from the physical models and the model training will be performed offline. After the model training, the prediction at a new process setting based on the trained models can be much faster than executing the physical models. This is beneficial to the real-time process optimization and control. In the following, we will explain the details of the proposed method.

# **Joint Tensor Decomposition**

Tensor decomposition is a powerful dimensional reduction technique. The basic idea of tensor decomposition is to approximate the high dimensional tensor with the product of low dimensional matrices and vectors. In the freeze nano printing, the droplet solidification time of the part will be decomposed into the multiplication of factorization matrices and a core tensor. In general, a third order tensor  $T \in \mathbb{R}^{I \times J \times K}$  can be factorized by CP decomposition [24]  $T \approx \tilde{T} = [\lambda; U, V, W] =$  $\sum_{r} \lambda_{r} u_{r} \circ v_{r} \circ w_{r}$ , where  $U \in R^{I \times R}$ ,  $V \in R^{J \times R}$ , and  $W \in R^{K \times R}$ are decomposition matrices,  $\lambda$  is a vector to specify the weight for each rank r, and the total rank is R (i.e.,  $r = 1, \dots, R$ ).  $\circ$  is the outer product. The total rank R can be determined so that the variation explained in the approximation tensor  $\tilde{T}$  is larger than a threshold percentage of the variation in the raw tensor T. The total rank R needed is usually a small number compared with the original dimensionality of the tensor. Such a selection approach is also widely used in determining the number of principal components in principal component analysis [25]. For our problem to model the droplet solidification time at various process settings, we want to use a compact representation of the raw tensor. Therefore, the decomposition matrices U, V and W for  $T_i$ 's at various process settings are shared (see Figure 3 for an illustration). We can therefore characterize the tensors with  $\lambda_i$  given the shared decomposition matrices U, V and W in the joint tensor decomposition [26]. In particular, the joint tensor decomposition can be solved via,

$$\min \frac{1}{n} \sum_{n} ||T_i - [\boldsymbol{\lambda}_i; U, V, W]||_F \tag{1}$$

 $\min \frac{1}{n} \sum_{n} ||T_i - [\lambda_i; U, V, W]||_F$  (1) where  $||\cdot||_F$  is the Frobenius norm, n is the number of samples, and  $\llbracket \cdot \rrbracket$  is the tensor product. The problem is solved with nonlinear least square (i.e., trust-region Quasi-Newton methods), where U, V and W are initialized with random matrices [27]. The rank R is selected to make sure the variation explained in the decomposition is larger than 99.5% of the total variation. After the joint tensor decomposition, other than modeling the raw tensor responses directly, the emulation problem can be simplified to model each  $\lambda_{i,r}$ 's in  $\lambda_i$  with a GP model,  $r = 1, \dots, R$ , respectively. This is because the non-zero entries in the core tensor only appear in the diagonal (Figure 3), and can be modeled independently.

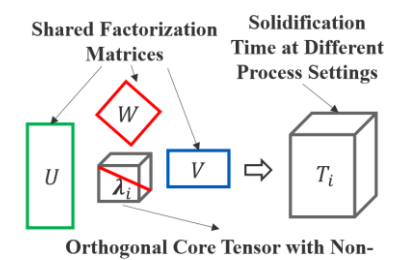


FIGURE 3. AN ILLUSTRATION OF THE JOINT TENSOR DECOMPOSITION

zero Entries in the Diagonal

# Gaussian Process (GP) Emulation

GP models can capture the nonlinear relationships in the data, and are widely used for physical model emulation and calibration [28]. For a certain rank r of the core tensors after the joint tensor decomposition, the  $\lambda_{i,r}$  in  $\lambda_i$  at the *i*-th sample can be modeled as

 $\lambda_{i,r}(\mathbf{x}) = m_{i,r}(\mathbf{x}) + \omega_{i,r}(\mathbf{x}) + \varepsilon_{i,r}(\mathbf{x}),$  (2) where  $\mathbf{x}$  contains the physical model inputs, such as layer thickness, droplet frequency, and the detailed values of these inputs are provided in Table 1.  $m_{i,r}(\mathbf{x}) = \mathbf{x}^T \boldsymbol{\beta}_{i,r}$  is the mean function capturing the mean effect of  $\mathbf{x}$  on  $\lambda_{i,r}$ , and  $\boldsymbol{\beta}_{i,r}$  is the model parameters for the mean effect;  $\omega_{i,r}(\mathbf{x})$  follows a GP  $\omega_{i,r}(\mathbf{x}) \sim GP\left(0, C_{i,r}(\mathbf{x}, \mathbf{x}')\right),$  where  $C_{i,r}(\mathbf{x}, \mathbf{x}') = \sigma_{i,r}^2 \exp\left(-\sum_j \phi_{i,r,j} \|x_j - x_j'\|\right)$  is the covariance function capturing the spatial relationship of samples.  $\phi_{i,r,j}$  is used to adjust the weight of each direction j while calculating the distance, and  $\sigma_{i,r}^2$  is a scaling parameter. For instance, based on the covariance function, the close by samples are highly correlated, whereas the far away samples tend to have lower correlation.  $\varepsilon_{i,r}(\mathbf{x}) \sim N(0, \tau_{i,r}^2)$  is the error term.

The unknown parameters in the GP model are  $\boldsymbol{\theta}_{i,r} = \{\boldsymbol{\beta}_{i,r}, \sigma_{i,r}^2, \boldsymbol{\phi}_{i,r,j}, \forall j\}$ , and can be learned from the Markov Chain Monte Carlo (MCMC) sampling from the posterior distribution [28],

$$p\left(\boldsymbol{\theta}_{i,r}|\lambda_{i,r}(\boldsymbol{x})\right) \propto p\left(\boldsymbol{\theta}_{i,r}\right) N\left(\lambda_{i,r}(\boldsymbol{x})|m_{i,r}(\boldsymbol{x}), C_{i,r}(\boldsymbol{x}, \boldsymbol{x}')\right) + \tau_{i,r}^2 I\right)$$
(3)

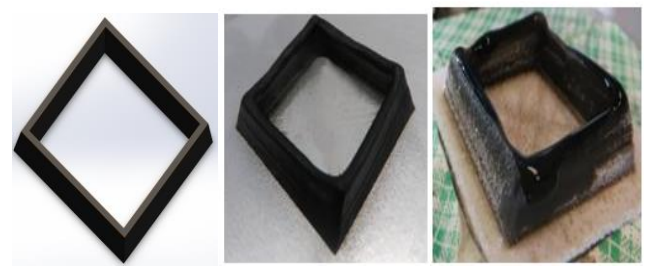
where  $p(\boldsymbol{\theta}_{i,r})$  is the prior distribution for the unknown parameters. The detailed specifications of  $p(\boldsymbol{\theta}_{i,r})$  will be provided in the Case Study section. After obtaining the posterior distribution, one can predict the  $\hat{\lambda}_{new,r}(\boldsymbol{x}_{new})$  at a new process setting  $\boldsymbol{x}_{new}$  [28].

# **Tensor Reconstruction and Comparison**

Up to this step, the tensor response of the droplet solidification time  $T_{new}$  of a new process setting  $\mathbf{x}_{new}$  can be predicted via tensor reconstruction. In particular,  $\hat{\lambda}_{new,r}(\mathbf{x}_{new})$ ,  $\forall r$  can be predicted from the individual GP models to form  $\hat{\lambda}_{new} = (\hat{\lambda}_{new,1}, \hat{\lambda}_{new,2}, \cdots, \hat{\lambda}_{new,R})$  in the core tensor. We can then reconstruct  $\hat{T}_{new} \approx [[\hat{\lambda}_{new}; U, V, W]]$  based on the U, V and W learned from the joint tensor decomposition. The predicted  $\hat{T}_{new}$  will be compared with the simulated  $T_{new}$  from the physical model for the emulation model evaluation.

#### **CASE STUDY**

As mentioned in the introduction, the accurate and efficient assessment of solidification time will affect the determination of the waiting time among layers, and subsequently affect the printed part quality. For instance, Figure 4 (b)-(c) shows the parts with proper and improper waiting times for the designed part in Figure 4 (a). In this section, we demonstrate the proposed framework for the accurate and efficient prediction of droplet solidification time in freeze nano printing.



a) Part CAD Model b) Proper Waiting c) Improper Waiting FIGURE 4. A COMPARISON OF PROPER AND IMPROPER WAITING TIME AMONG LAYERS

To demonstrate the proposed framework, we simulate a single layer freeze nano printing part with 10 by 10 droplets based on the physical models in [12]. Figure 5 shows the simulation setup. The deposited droplets have an initial temperature of 5 °C and are deposited based on the path specified in Figure 5 (c). After the ejection (Figure 5 (a)), the droplets solidify in a short time due to the heat conduction with the heat sink (at -20 °C) under build bed and heat convection with the ambient (Figure 5 (b)). The corresponding droplet solidification time (time required for a droplet to cool down from 5 °C to -19 °C in this case) is summarized as shown in Figure 5 (c). In the simulation, we vary six process parameters that will affect the thermal distribution. The names and ranges (lower and upper bounds) of these parameters are shown in Table 1. We generate 60 simulation runs from the physical model. In these simulation runs, the process settings are determined by a Latin hypercube sampling based space filling design [29].

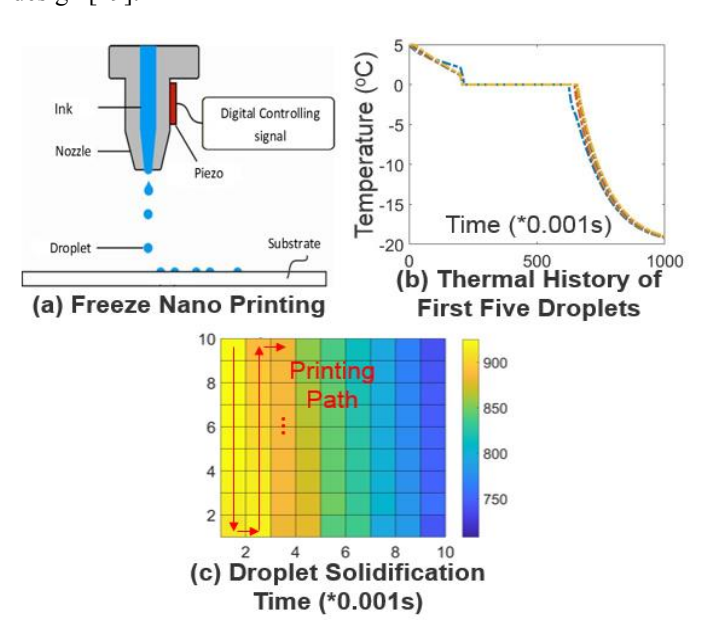


FIGURE 5. SIMULATION SETUP (a) DROPLET EJECTION FROM FREEZE NANO PRINTING (b) INDIVIDUAL DROPLET THERMAL HISTORY (c) SUMMARIZED DROPLET SOLIDIFICATION TIME

TABLE 1. SIMULATION PARAMETERS AND RANGES

IDs	Parameters	Lower Bounds	Upper Bounds
$X_1$	Specific heat $J/(kg \cdot K)$	3350	3450
$X_2$	Frequency (Hz)	50	500
$X_3$	Density (kg/m <sup>3</sup> )	1000	1300
$X_4$	Layer thickness (mm)	0.1	0.6
<i>X</i> <sub>5</sub>	Interface heat transfer coefficient $(W/m^2 \cdot K)$	200	500
<i>X</i> <sub>6</sub>	Element heat transfer coefficient $(W/m^2 \cdot K)$	50	150

We apply the proposed framework to the solidification time at all process settings. During the model training, the simulated samples are divided into five randomly generated and equally sized folds for cross validation (CV). In iterations, four out of the five folds are used for model training, and the remaining fold is used for model testing. And this training and testing iterations are repeated for five times. During the model training, the rank in the joint tensor decomposition varies from 10%, 20% up to 90% of the total tensor dimension, and the final rank is selected to keep the proportion of explained variance not less than 99.5% of the total variance of the droplet solidification time in any process settings, i.e.,  $\max_{i} \|\lambda_{i}; U, V, W\|_{F} / \|T_{i}\|_{F} \ge 99.5\%$ . For the joint tensor decomposition in our case, the selected rank R is 3 or 4, depending on the training and testing CV folds. After the determination of tensor rank R and the learning of the factorization matrices U, V and W, these factorization matrices are applied to the samples in the left out CV fold to learn the core tensors. The corresponding core tensor entries will be used as the testing data for the GP model evaluation.

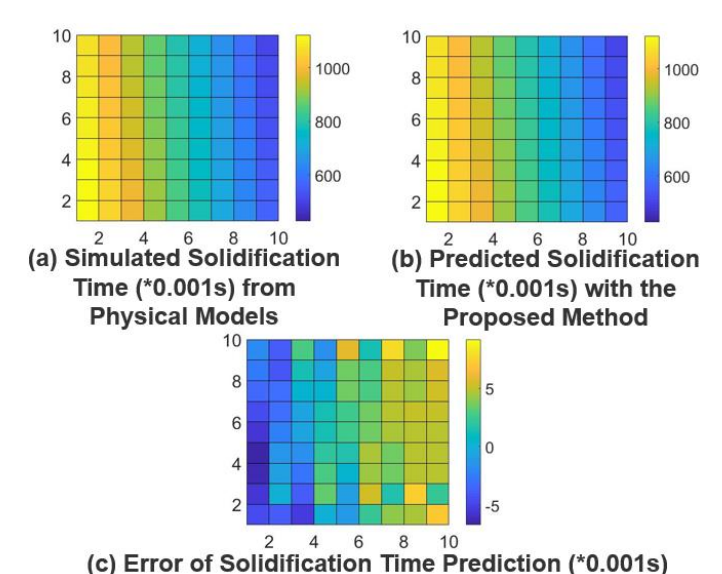


FIGURE 6. Comparison of Solidification Time

Simulated from Physical Models and Predicted from the **Proposed Method** 

For the GP model training in Eq. (2), we have each core tensor entries (e.g., the r-th entry  $\lambda_{i,r}$ ,  $\forall i$ ) in the training data as the outputs, and the corresponding process settings as inputs x. In Eq. (2), the prior distributions for  $\beta_{i,r,j}$ ,  $\tau_{i,r}$  and  $\sigma_{i,r}$  are set as Gaussian, and the prior distribution for  $\phi_{i,r,i}$  is set as inverse gamma. During the MCMC estimation of these GP model parameters, we have in total 10,000 iterations. Among these 10,000 iterations, 5,000 iterations are used for burn-in (i.e., the burn-in iterations will be discarded to make sure the posterior distribution is stable). After the burn-in, the MCMC mixed well, which indicates that the posterior distributions converge. We then use the last MCMC 5,000 iterations for the model prediction at a certain process setting. In particular, we calculate the mean of the predicted  $\hat{\lambda}_{new,r}(\mathbf{x}_{new})$ 's from 5,000 posterior draws. The above procedures are repeated for all  $r = 1, \dots, R$ . We then organize the predicted  $\hat{\lambda}_{new} =$  $(\hat{\lambda}_{new,1}, \hat{\lambda}_{new,2}, \cdots, \hat{\lambda}_{new,R}),$ and perform the tensor reconstruction introduced in the Proposed Method section.

Figure 6 shows a comparison of the simulated, predicted and the prediction error for the solidification time at a random process setting (note that the color intensity shows the number of computation steps in the physical model, and the step size is 0.001s). From the figures, the proposed framework can effectively predict the solidification time.

To more systematically assess the modelling approach, we summarize the joint tensor decomposition rank R, the Normalized Root Mean Square Error (NRMSE) prediction error, and computation time in Table 2. The NRMSE is calculated via  $\sum_{i} ||T_i - \widehat{T}_i||_F / \sum_{i} ||T_i||_F$ , where  $T_i$  is the true simulated solidification time, and  $\widehat{T}_t$  is the predicted solidification time. From Table 2, the proposed framework can capture the variations in the solidification time with a small number of rank, and the GP model can have a relatively small NRMSE. The model prediction for a new sample can be performed in around 2 seconds, which is much faster than running the physical models (which can take minutes to run even for a simple shape in this study), and can facilitate the real-time process optimization and control.

TABLE 2. JOINT TENSOR DECOMPOSITION RANK, NRMSE AND COMPUTATIONAL TIME SUMMARY

	Sample Size 60		
	Rank	NRMSE	Time (s)
Fold 1	3	11.79%	295.49
Fold 2	3	14.72%	256.09
Fold 3	4	11.31%	334.01
Fold 4	3	8.39%	264.01
Fold 5	3	11.72%	252.42

#### CONCLUSION AND DISCUSSION

In energy 3D printing, the droplet solidification time is critical for the part integrity and property. The droplet solidification time is dependent on the process settings, and is impractical to be investigated from a trial-and-error approach

due to the high material cost in energy 3D printing. The physical model based simulation of droplet solidification time is an alternative to the problem. However, the computation of the physical model can take time, which prevents their utilization for the real-time prediction and process optimization. Therefore, we explore machine learning methods to address the prediction of the high dimensional solidification time for future real-time process optimization and control. In particular, we integrate joint tensor decomposition, Gaussian process models and the physical model outputs in our framework. The novelty of this paper is that the matrix or tensor responses can be effectively represented by low dimensional vectors and matrices, and the computation can be performed separately for the orthogonal core tensor based on GP models. It is shown that the proposed framework can build an efficient and accurate emulator for the prediction of the solidification time under new process settings.

There are several areas of research that we want to explore following this work: 1) we will further increase the prediction accuracy. One strategy is to increase the simulation data sample size. However, this will significantly affect the model training speed since the complexity of GP model is  $O(n^3)$ . We will explore accelerated models, such as nearest-neighbor Gaussian process for the tensor responses emulation. 2) We will consider a unified framework for the joint tensor decomposition and GP models, to avoid the potential sub-optimality when performing them separately. 3) We will compare the proposed approach with other models addressing the tensor responses, such as tensor regression. 4) Before implementing the proposed framework for the real-time process control and optimization, it is necessary to validate the model with the physical experiments. Therefore, we will take the thermal measurement from the freeze nano printing process and perform the model calibration. 5) We will ultimately use the calibrated model for the process optimization and control, so that we can adjust the waiting time and process parameters during the printing.

#### REFERENCES

- [1] A. M. Zamarayeva, A. E. Ostfeld, M. Wang, J. K. Duey, I. Deckman, B. P. Lechêne and A. C. Arias, "Flexible and stretchable power sources for wearable electronics," *Science Advances*, Vol. 3, No. 6, pp. e1602051, 2017.
- [2] L. Nyholm, G. Nyström, A. Mihranyan and M. Strømme, "Toward flexible polymer and paper-based energy storage devices.," *Advanced Materials*, Vol. 23, No. 33, pp. 3751-3769, 2011.
- [3] N. R. Council, Meeting the energy needs of future warriors, National Academies Press, 2004.
- [4] M. Beidaghi and Y. Gogotsi, "Capacitive energy storage in micro-scale devices: recent advances in design and fabrication of micro-supercapacitors," *Energy & Environmental Science*, Vol. 7, No. 3, pp. 867-884, 2014.
- [5] B. Berman, "3-D printing: The new industrial revolution," *Business Horizons*, Vol. 55, No. 2, pp. 155-162, 2012.

- [6] K. Fu, Y. Wang, C. Yan, Y. Yao, Y. Chen, J. Dai and Z. Wang, "Graphene oxide-based electrode inks for 3D-printed lithium-ion batteries," *Advanced Materials*, Vol. 28, No. 13, pp. 2587-2594, 2016.
- [7] C. Zhu, T. Liu, F. Qian, T. Y. J. Han, E. B. Duoss, J. D. Kuntz and Y. Li, "Supercapacitors based on three-dimensional hierarchical graphene aerogels with periodic macropores," *Nano Letters*, Vol. 16, No. 6, pp. 3448-3456, 2016.
- [8] M. Areir, Y. Xu, D. Harrison and J. Fyson, "3D printing of highly flexible supercapacitor designed for wearable energy storage," *Materials Science and Engineering*, Vol. B, No. 226, pp. 29-38, 2017.
- [9] Q. Zhang, F. Zhang, S. P. Medarametla, H. Li, C. Zhou and D. Lin, "3D printing of graphene aerogels," *Small*, Vol. 12, No. 13, pp. 1702-1708, 2016.
- [10] F. Zhang, M. Wei, V. V. Viswanathan, B. Swart, Y. Shao, G. Wu and C. Zhou, "3D printing technologies for electrochemical energy storage," *Nano Energy*, Vol. 40, pp. 418-431, 2017.
- [11] H. Bikas, P. Stavropoulus and G. Chryssolouris., "Additive manufacturing methods and modelling approaches: a critical review," *The International Journal of Advanced Manufacturing Technology*, Vol. 83, No. (1-4), pp. 389-45, 2016.
- [12] G. Zhao, C. Zhou and D. Lin, "Thermal analysis on directional freezing of nano aqueous suspensions in graphene aerogel 3D printing process," *ASME 2016 11th International Manufacturing Science and Engineering Conference*, pp. V003T08A011-V00, 2016.
- [13] P. Yuan and D. Gu, "Molten pool behavior and its physical mechanism during selective laser melting of TiC/AlSi10Mg nanocomposites: simulation and experiments," *Journal of Physics D: Applied Physics*, Vol. 48, No. 3, pp. 035303, 2015.
- [14] H. C. Wu, H. J. Lin, Y. C. Kuo and W. S. Hwang, "Simulation of droplet ejection for a piezoelectric inkjet printing device," *Materials Transactions*, Vol. 45, No. 3, pp. 893-899, 2004.
- [15] K. Sun, T. S. Wei, B. Y. Ahn, J. Y. Seo, S. J. Dillon and J. A. Lewis, "3D printing of interdigitated Li-Ion microbattery architectures," *Advanced Materials*, Vol. 25, No. 33, pp. 4539-4543, 2013.
- [16] G. Tapia, A. H. Elwany and H. Sang, "Prediction of porosity in metal-based additive manufacturing using spatial Gaussian process models," *Additive Manufacturing*, Vol. 12, pp. 282-290, 2016.
- [17] Q. Huang, J. Zhang, A. Sabbaghi and T. Dasgupta, "Optimal offline compensation of shape shrinkage for three-dimensional printing processes," *IIE Transactions*, Vol. 47, No. 5, pp. 431-441, 2015.

- [18] M. S. Tootooni, A. Dsouza, R. Donovan, P. K. Rao, Z. J. Kong and P. Borgesen, "Classifying the dimensional variation in additive manufactured parts from laser-scanned three-dimensional point cloud data using machine learning approaches," *Journal of Manufacturing Science and Engineering*, Vol. 139, No. 9, pp. 091005, 2017.
- [19] F. Liravi, R. Darleux and E. Toyserkani, "Additive manufacturing of 3D structures with non-newtonian highly viscous fluids: finite element modeling and experimental validation," *Additive Manufacturing*, Vol. 13, pp. 113-123, 2017.
- [20] J. Li, R. Jin and Z. Y. Hang, "Integration of physically-based and data-driven approaches for thermal field prediction in additive manufacturing," *Materials & Design*, Vol. 139, pp. 473-485, 2018.
- [21] H. Yan, K. Paynabar and M. Pacella, "Structured point cloud data analysis via regularized tensor regression for process modeling and optimization," *Technometrics*, pp. 1-36, 2018.
- [22] M. S. Tootooni, A. Dsouza, R. Donovan, P. K. Rao, Z. J. Kong and P. Borgesen, "Assessing the geometric integrity of additive manufactured parts from point cloud data using spectral graph theoretic sparse representation-based classification," In ASME 2017 12th International Manufacturing Science and Engineering Conference collocated with the JSME/ASME 2017 6th International Conference on Materials and Processing, pp. V002T01A042-V002T01A042, 2017.
- [23] H. Yan, K. Paynabar and J. Shi, "Image-based process monitoring using low-rank tensor decomposition," *IEEE*

- *Transactions on Automation Science and Engineering*, Vol. 12, No. 1, pp. 216-227, 2015.
- [24] N. D. Sidiropoulos, L. D. Lathauwer, X. Fu, K. Huang, E. E. Papalexakis, C. Faloutsos, "Tensor decomposition for signal processing and machine learning," *IEEE Transactions on Signal Processing*, Vol. 65, No. 13, pp. 3551-3582, 2017.
- [25] S. Zhou and J. Jin, "Automatic feature selection for unsupervised clustering of cycle-based signals in manufacturing processes," *IIE Transactions*, Vol. 37, No. 6, pp. 569-584, 2005.
- [26] R. C. Farias, J. E. Cohen and P. Comon, "Exploring multimodal data fusion through joint decompositions with flexible couplings," *IEEE Transactions on Signal Processing*, Vol. 64, No. 18, pp. 4830-4844, 2016.
- [27] N. Vervliet, O. Debals and L. De Lathauwer, "Tensorlab 3.0 -- numerical optimization strategies for large-scale constrained and coupled matrix/tensor factorization," *In 50th Asilomar Conference on Signals, Systems and Computers*, pp. 1733-1738, 2016.
- [28] C. E. Rasmussen, "Gaussian processes in machine learning," *Advanced Lectures on Machine Learning*, pp. 63-71, 2004.
- [29] T. J. Santner, B. J. Williams and W. I. Notz, "The design and analysis of computer experiments," *Springer Science & Business Media*, 2013.